Available online at www.sciencedirect.com
SCIENCE DIRECT®
PERGAMON
International Journal of Multiphase Flow 29 (2003) 1283–1309
International Journal of Multiphase Flow
www.elsevier.com/locate/ijmulflow

Tuning of parameters in a two-phase flow model using an ensemble Kalman filter

R.J. Lorentzen [a,*], G. Nævdal [a], A.C.V.M. Lage [b]

[a] *RF-Rogaland Research, Thormøhlensgt. 55, N-5008 Bergen, Norway*
[b] *Petrobras, Research and Development center (CENPES), Cidade Universitária, Q.7 Ilha do Fundão 21949-900, Rio de Janeiro, Brazil*

Received 1 September 2002; received in revised form 24 April 2003

Abstract

A new methodology for online tuning of model parameters in a two-phase flow model by taking into account measured data is presented. Important model parameters are tuned using the ensemble Kalman filter. The present study is motivated by applications in underbalanced drilling, although the idea of using the ensemble Kalman filter in tuning of model parameters should be of interest in a wide area of applications. A description of modeling of the two-phase flow in the well is presented, as well as the implementation of the ensemble Kalman filter. The performance of the filter is studied, both using synthetic and experimental data.

Keywords: Ensemble Kalman filter; Two-phase flow; Well-flow modeling

1. Introduction

The development of increased computer power and advances in measuring techniques give new opportunities in online tuning of complex models. Within atmospheric and oceanic literature there has been a strong interest in data assimilation during the last decade. This has resulted in the adaption of Kalman filter techniques to large-scale non-linear models. The use of these Kalman filter techniques within other areas seems to be a promising area of research. In this paper we will

* Corresponding author. Fax: +47-55543860.
E-mail address: rolf.lorentzen@rf.no (R.J. Lorentzen).

0301-9322/03/$ - see front matter
doi:10.1016/S0301-9322(03)00088-0

demonstrate how the ensemble Kalman filter can be used to tune model parameters of a two-phase flow system.

Modeling of two-phase flow is a difficult task, and simplifications have to be done. In the present application we study two-phase flow in wells. As a simplification we treat this as an one dimensional problem using a model obtained from cross sectional averaging of the Navier–Stokes equations, replacing second order diffusion terms by empirical correlations (including model parameters) which are flow regime dependent. These correlations are obtained from laboratory experiments conducted in different surroundings than real full-scale facilities, and possibilities of inaccuracies due to system dependencies does therefore exist. It is crucial to use all available information to tune the model parameters, as their values have large impact on the behaviour of the system. In particular it is useful to do online tuning, to exploit the current measurements. We show that such tuning can be done using a Kalman filter approach by including model parameters in the state vector of the system. The parameters are then updated as new measurements become available. In this paper we will show that the model parameters we chose are updated satisfactorily, leading to improved forecasts of the future flow.

Several Kalman filter techniques have been developed to work with large-scale non-linear system. We have implemented the ensemble Kalman filter, first introduced by Evensen (1994). The ensemble Kalman filter is based on a Monte-Carlo approach, using an ensemble of model representations to build up the necessary statistics. The ensemble Kalman filter is easy to implement and handles strong non-linearities better than other known Kalman filter techniques for large-scale problems (Verlaan and Heemink, 2001). There is a lot of ongoing work within meteorology and oceanography using Kalman filter techniques, both using ensemble Kalman filter and other techniques. Some recent works in this direction are (e.g. Verlaan and Heemink, 2001; Anderson, 2001; Hamil et al., 2001). We refer to these works, and the works cited therein for those who are interested in the state of the art of the research on Kalman filter for large-scale non-linear models.

To our knowledge, there has been a limited number of applications on ensemble Kalman filter techniques for tuning model parameters. In the above mentioned works, the focus is on improving the estimate of the state variables, although the tuning of one model parameter is discussed using an ensemble adjustment Kalman filter in Anderson (2001). (The ensemble adjustment Kalman filter is a slight modification of the ensemble Kalman filter.) Here we will use the ensemble Kalman filter to tune nine model parameters. The promising result of the present work has motivated further studies in using the ensemble Kalman filter for tuning of model parameters. In Nævdal et al. (2002a,b) the tuning of the permeability field in a porous media model is studied.

The setup of our model is motivated by applications within underbalanced drilling. The ensemble Kalman filter was used for tuning of the model parameters in Lorentzen et al. (2001a). In that study, using both synthetic and full-scale experimental data, we showed that the tuning improved the fitting of the data, and that more reliable predictions were obtained. Here we both present results from a study on the robustness of the methodology, using synthetic data, as well as some more results with full-scale experimental data. An alternative to using the ensemble Kalman filter to tune the model parameters is to use a least square approach. This technique was exploited in Lorentzen et al. (2001b). The least square approach is, however, more computationally demanding, and seems therefore not to be suitable to online tuning (Lorentzen, 2002).

We will study the robustness of the ensemble Kalman filter using synthetic data. Measurements are generated synthetically using different sets of model parameters. It is shown that by using the ensemble Kalman filter the model parameters are tuned so that the measurements are fitted, and reasonable predictions are obtained, thereby giving evidence for the robustness of the ensemble Kalman filter. Although the final judgment of the methodology has to be based on its performance on real data, the use of synthetic data give some more possibilities in judging the results. After studying the robustness of the approach using synthetic data, we present results using a set of experimental data.

The paper is organized as follows. In Section 2 the physical model is presented. In Section 3 the implementation of the ensemble Kalman filter is presented. For the convenience of the reader, a self-contained presentation of the ensemble Kalman filter in general is included. In Section 4 we discuss the details of the chosen variables (including different covariance matrices) in the setup of the filter for the present application and present the results.

2. Dynamic model

A model describing one-dimensional two-phase flow in pipelines consists of non-linear partial differential equations describing mass, momentum and energy balances for each of the phases (see e.g. Ishii, 1975). This model is obtained from cross sectional averaging of the Navier–Stokes equations and replacing second order diffusion terms by empirical correlations which are flow regime dependent. The dynamics of multiphase flow are determined by these balance equations which involve complicated terms for interface exchanges of mass, momentum and energy. In addition, wall friction and volumetric forces like gravity are highly responsible for the development of the flow.

The focus of this work is the application of filter techniques rather than a detailed fluid description, and we limit ourselves to consider gas–liquid flow in vertical wells. We assume that no mass enters or leaves the system through the pipe walls, and we neglect mass transfer between the phases. The simplified mass conservation equations are then written

$$\frac{\partial}{\partial t}(\alpha_k A \rho_k) + \frac{\partial}{\partial s}(\alpha_k A \rho_k v_k) = 0, \quad k = \mathrm{l}, \mathrm{g}, \tag{1}$$

where l, g represents the liquid and gas phase respectively, t denote the time variable, α is the volume fraction, A is cross-section area, ρ is the density, s denote the coordinate along the pipe and v is the velocity.

The fundamental two-phase model consists of separate momentum conservation equations for each phase, and includes complicated terms related to phase interaction. It is however a common practice in two-phase modeling to add the momentum equations together, which causes the difficult phase interaction terms to cancel (see Fjelde, 2000; Faille and Heintzé, 1999; Pauchon et al., 1994). This results in the following simplified equation for the mixture phase (drift flux formulation):

$$\frac{\partial}{\partial t} A(\alpha_\mathrm{l}\rho_\mathrm{l}v_\mathrm{l} + \alpha_\mathrm{g}\rho_\mathrm{g}v_\mathrm{g}) + \frac{\partial}{\partial s} A(\alpha_\mathrm{l}\rho_\mathrm{l}v_\mathrm{l}^2 + \alpha_\mathrm{g}\rho_\mathrm{g}v_\mathrm{g}^2) + A\frac{\partial}{\partial s}p = -A(K - \rho_\mathrm{mix} g \sin\theta), \tag{2}$$

where p is the pressure, K is a friction pressure loss term, θ is the well inclination and $\rho_{\text{mix}} = \rho_{\text{g}}\alpha_{\text{g}} + \rho_{\text{l}}\alpha_{\text{l}}$ is the mixture density. We further assume that there is no heat exchange in the fluid, which makes the energy conservation equation redundant (isentropic flow).

The stated governing partial differential equations for the two-phase flow are insufficient to completely describe the physical processes involved. There are more unknowns than equations and thus closure conditions are required. The missing information in the mixture momentum equation must be replaced by empirical closure relations which provide information about phase velocities and pressure loss terms. These relations consist of complicated time-dependent equations (see e.g. Franca and Lahey, 1992; Bendiksen, 1984; Cassaude et al., 1989; Lage, 2000) and include several parameters which are only approximately known. Inaccuracies in these parameters relates to system dependencies such as complex fluid properties, geometry, impurities in the fluids, flow regime (laminar/turbulent) and unknown pipe properties. The object of this paper is to show how measurements can be used to improve these parameters, leading to better forecasts of the two-phase flow. We consider one set of simple closure relations for downward two-phase flow in the drillstring, and a more sophisticated mechanistic model for upward two-phase flow in the annulus. This model takes into account the complex and regime-dependent relations for the phase velocities and pressure loss terms.

In addition to closure relations describing phase velocities it is necessary to specify thermodynamic relations, generally derived by assuming a system in thermodynamic equilibrium (PVT-models). In this work, the PVT-models are obtained by assuming an ideal gas law and a liquid density model with fixed compressibility. It is also necessary to provide boundary conditions for the system. In this context, the flow rates are assumed to be known at the inlet, and the pressure is assumed to be given at the outlet.

2.1. Closure relations for downward two-phase flow in the drillstring

In the standard drift-flux approach, the closure of the system is achieved by specifying a slip model between the phases:

$$v_{\text{g}} = C_{0,d}(\alpha_{\text{g}}v_{\text{g}} + \alpha_{\text{l}}v_{\text{l}}) + C_{1,d} = C_{0,d}v_{\text{mix}} + C_{1,d}. \tag{3}$$

In addition, it is necessary to provide an appropriate model for the frictional pressure loss term in the momentum equation. A frequently used expression for this term is

$$K = C_{2,d}\frac{2f}{D}\rho_{\text{mix}}v_{\text{mix}}^2, \tag{4}$$

where f is a known flow dependent friction factor, D is the pipe diameter and $v_{\text{mix}} = v_{\text{g}}\alpha_{\text{g}} + v_{\text{l}}\alpha_{\text{l}}$ is the mixture velocity. In Eqs. (3) and (4), the factors $C_{0,d}$, $C_{1,d}$ and $C_{2,d}$ are assumed to be given parameters, and are among the parameters which are tuned by the filter technique described in subsequent sections.

2.2. Mechanistic model for upward two-phase flow in the annulus

Mechanistic models have become quite popular for describing steady-state two-phase flow in producing wells. The mechanistic models provide information about flow patterns, pressure drops and phase velocities:

$$M(D_1, D_2, \rho_l, \rho_g, \tau, \mu_l, \mu_g, q_{mix}, \alpha_g, \alpha_l) \rightarrow (v_g, v_l, \text{ pressure loss}), \tag{5}$$

where D_1 and D_2 are the inner and outer diameter respectively, μ_l and μ_g are the viscosities for the liquid and gas phase, τ is the interfacial tension and $q_{mix} = \rho_g \alpha_g v_g + \rho_l \alpha_l v_l$ is the mixture momentum. Furthermore, it is possible to integrate these mechanistic steady-state procedures into fully dynamic two-phase flow models to provide the necessary information regarding phase velocities and pressure loss terms (see e.g. Pauchon et al., 1994; Lage et al., 2000a,b; Bendiksen et al., 1991). We have implemented a recently developed mechanistic model for two-phase flow in annulus, described in the work by Lage (2000), Lage and Time (2000).

A mechanistic model consists of basically two parts, where one part is composed of criteria for predicting the flow pattern. The other part consists of models for treating each specific pattern. The framework developed by Taitel and Barnea (1983) is the basis for the definition of the transition criteria. They considered five different flow configurations (bubble, dispersed bubble, slug, churn and annular) for upward two-phase flow in pipes and formulated boundaries between them. Although the implemented method include all five configurations, we limit the following presentation to bubble flow and slug flow. These flow regimes are dominant in the examples we have considered, and parameters related to these regimes are tuned by the ensemble Kalman filter presented in Section 3.

2.2.1. Bubble flow model

Harmathy (1960) proposed

$$v_{0\infty} = C_{1,b} 1.53 \left[\frac{(\rho_l - \rho_g) g \tau}{\rho_l^2} \right]^{0.25} \tag{6}$$

for the rise velocity of a single bubble rising in an infinite medium, with $C_{1,b} = 1$. It is only a function of the physical properties of gas and liquid. However, Wallis (1969) proposed that for a bubble rising in a swarm of bubbles, Eq. (6) should be corrected by

$$v_0 = v_{0\infty}(1 - \alpha_g)^n, \tag{7}$$

where the exponent n is assumed to be known.

The slippage between gas and liquid phases is the key aspect to be considered for determining the flow parameters. As suggested by Papadimitriou and Shoham (1991), the slip velocity is defined as

$$v_g = v_0 + C_{0,b} v_{mix}.$$

This equation is used to calculate the unknown phase velocities. The friction pressure loss is given by

$$K = C_{2,b}\frac{2f}{D_h}\rho_{\mathrm{mix}}v_{\mathrm{mix}}^2,$$

where D_h is the difference between the outer and inner diameter. The parameters $C_{0,b}$, $C_{1,b}$ and $C_{2,b}$ are added to the vector of parameters which is tuned by the ensemble Kalman filter.

2.2.2. Slug flow model

Fig. 1 presents a schematic diagram of an idealized slug unit in an annulus. Large Taylor bubbles of length l_{tb}, move upward, and Kelessidis and Dukler (1989) proposed the following expression for the translational velocity v_{tb}:

$$v_{\mathrm{tb}} = C_{0,s}v_{\mathrm{mix}} + C_{1,s}0.35\sqrt{g(D_1 + D_2)},$$

with $C_{0,s} = 1.2$ and $C_{1,s} = 1$. The Taylor bubbles are followed by liquid slugs containing small, uniformly distributed bubbles with an average gas fraction $\alpha_{\mathrm{g,ls}} = 0.2$. By integrating over the entire slug unit, the following equation for the gas velocity is obtained:

$$v_{\mathrm{g}} = v_{\mathrm{tb}} - \frac{\alpha_{\mathrm{g,ls}}}{\alpha_{\mathrm{g}}}(v_{\mathrm{tb}} - v_{\mathrm{g,ls}}),$$

where ls indicates the value of the flow variable in the liquid slug zone. The gas velocity in the liquid slug zone ($v_{\mathrm{g,ls}}$) is found by using v_{mix} and the equations derived for bubble flow. The liquid velocity is then found by substituting v_{g} in the expression for q_{mix}. A detailed discussion of modeling of slug flow, and choice of parameters values, is found in Bendiksen et al. (1996).

A mass balance calculation for the slug unit provides values for the length of the slug unit and the length of the liquid slug. All the parameters are then available for the pressure drop calculations. The friction pressure gradient is evaluated in the liquid slug zone as

$$K = C_{2,s}\frac{2f}{D_h}\rho_{\mathrm{mix}}v_{\mathrm{mix}}^2\frac{l_{\mathrm{ls}}}{l_{\mathrm{su}}}.$$

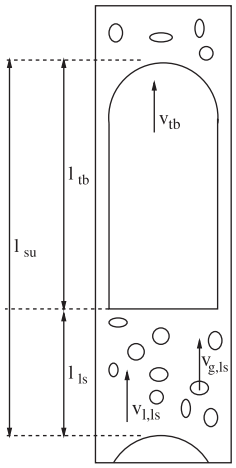

Fig. 1. Slug flow structure.

The parameters $C_{0,s}$, $C_{1,s}$ and $C_{2,s}$ complete the list of parameters which are tuned by the ensemble Kalman filter.

2.2.3. Transition regime

In order to ensure a smooth development of the two-phase flow, the mechanistic model uses a transition regime between the bubble flow regime and the slug flow regime. The transition regime is modeled by performing interpolations of the flow variables resulting from the bubble flow model and the slug flow model.

2.3. Numerical scheme

The non-linear and coupled characteristic of the drift-flux model makes it impossible to solve the equations analytically, and a numerical solution strategy is required. The aim of the numerical solver is to compute accurate and stable approximations of the flow variables (e.g. pressure, velocity, volume fractions etc.). Numerical methods replace the continuous problem represented by the Eqs. (1) and (2) by a finite set of discrete values.

The drift-flux model can be written as a system of conservation laws which has been analyzed by Théron (1989) and Gavage (1991). The model was shown to be hyperbolic in a physically reasonable region of parameters and three distinct and real eigenvalues were obtained under the main assumption that the liquid phase was considered incompressible. Two of the eigenvalues (λ_1 and λ_3) correspond to rapid pressure waves propagating in the upstream and downstream direction of the fluid flow, while the last eigenvalue (λ_2) is associated to gas volume waves and equal to the gas velocity. The eigenvalues corresponding to the pressure pulses are generally 10–100 times bigger than the eigenvalue corresponding to the mass transport, i.e. $|\lambda_1|, |\lambda_3| \gg |\lambda_2|$.

We have chosen a numerical method which follows the idea described in Frøyen et al. (2000). It is a semi-implicit solution strategy which treats the acoustic signals associated with λ_1 and λ_3 implicit while maintaining the explicit treatment of the mass transport. The time step is thus limited by the time interval the mass transport signal use to traverse a grid block. Some of the solution details are thus sacrificed to increase computational efficiency. This method has been tested against experimental data in an underbalanced drilling scenario in Lage et al. (2000b).

3. Estimation theory

In the models presented in Section 2 there are some influential parameters which are uncertain. Improved knowledge on the value of these parameters leads to significantly better predictions of the system behavior. There are several approaches available to fit these parameters. In Lorentzen et al. (2001a) the parameters were fitted using the ensemble Kalman filter. A minimization between the model output and measurements using a least squares approach was pursued in Lorentzen et al. (2001b). Here, we will continue the studies from Lorentzen et al. (2001a), and study the robustness of the ensemble Kalman filter in the tuning of the model parameters, in addition to presenting more results using experimental data.

The Kalman filter was initially developed for the discrete-data linear filtering problem. An introduction to the general idea of the Kalman filter can be found in Maybeck (1979). As the

measurements become available, they are used to estimate the state of the process. (The states of the system are the time dependent variables.) It is straightforward to extend the state variables with model parameters, by treating the model parameters as time dependent variables. The Kalman filter has been the subject of extensive research, and several adaptions to non-linear systems have been developed. A recent approach which has been applied successfully for large-scale non-linear models within oceanographic modeling is the ensemble Kalman filter, first introduced in Evensen (1994).

For the convenience of the reader we present our implementation of the ensemble Kalman filter. The filter can be divided in two steps, a forecast step and an analysis step. In the forecast step the state of the system is updated by solving the dynamic model as described in Section 2. In the analysis step the state of the model is updated to take into account the measurements. The state vector after running the forecast step is denoted by Ψ_k^{f}, the state vector after the analysis step by Ψ_k^{a}.

The ensemble Kalman filter is based on a Monte-Carlo approach, using an ensemble of model representations to evaluate the necessary statistics. We have used 100 members in the ensemble. We selected this size of the ensemble since an ensemble size of this order have been found to be sufficient for much larger atmospheric models (Houtekamer and Mitchell, 1998). The influence of the size of the ensemble on the performance of the ensemble Kalman filter for this application is a topic worthwhile further research. The experience in using the ensemble Kalman filter for parameter estimation and also for tuning of multiphase flow models is limited.

The forecast step consists in running the model (i.e. the simulator developed as described in Section 2.3), which we denote by $\mathbf{f}$, one time step for each member of the ensemble. For the i'th member of the ensemble at time step k, we denote the forecast state vector by $\Psi_{k,i}^{\mathrm{f}}$ and the analyzed state by $\Psi_{k,i}^{\mathrm{a}}$. In the forecast step the simulator is run from the current time (say timestep $k-1$) to the point in time where the next measurement becomes available (timestep k). The simulator is run once for each member of the ensemble using the analyzed state $\Psi_{k-1,i}^{\mathrm{a}}$ as initial value. In addition to the updating of the state given by the simulator, random model noise is added. This gives the equation

$$\Psi_{k,i}^{\mathrm{f}} = \mathbf{f}(\Psi_{k-1,i}^{\mathrm{a}}) + \mathbf{e}_{k,i}^{m}, \tag{8}$$

where $\mathbf{e}_{k,i}^{m} \sim N(\mathbf{0}, \mathbf{Q}_k)$. The notation $\mathbf{e}_{k,i}^{m} \sim N(\mathbf{0}, \mathbf{Q}_k)$ denotes that the model noise is generated by drawing realizations from a Gaussian distribution with zero mean and covariance matrix $\mathbf{Q}_k$. Here the distribution of the model noise may be time dependent. The time dependence of the distribution of the model noise is due to the fact that the covariance matrix Q may be time dependent.

The filter is initialized by generating an initial ensemble. This is done by specifying a mean value, $\overline{\Psi_0^{\mathrm{a}}}$ and a covariance matrix, $\mathbf{Q}_0$ of the initial ensemble. The mean value of the initial ensemble should preferably be a good estimate of the initial true state. The members of the ensembles are then drawn randomly assuming a Gaussian distribution,

$$\Psi_{0,i}^{\mathrm{a}} = \overline{\Psi_0^{\mathrm{a}}} + \mathbf{e}_{0,i}^{m}, \tag{9}$$

where $\mathbf{e}_{0,i}^{m} \sim N(\mathbf{0}, \mathbf{Q}_0)$.

The analyzed state at time step k is computed by taking into account the measurement vector at time step k. We assume that there is a linear relationship between the measurements, $\mathbf{d}_k$, and the states, Ψ_k, expressed by the equation

$$\mathbf{d}_k = \mathbf{H}\Psi_k. \tag{10}$$

The above equation refers to an idealized situation with no noise and no representation error in the measurements. We assume that these effects can be expressed by a Gaussian random variable with zero mean and covariance matrix $\mathbf{R}_k$. The index k is included since the covariance matrix of the measurement noise may be time dependent, for instance when the measurement accuracy is given as a relative accuracy. We assume that there is no correlation in the noise of measurements taken at different time steps.

As pointed out in Burgers et al. (1998) it is necessary to define new observations for proper error propagation in the ensemble Kalman filter. The actual measurement $\mathbf{d}_k$ serves as the reference observation. For each member of the ensemble an observation vector $\mathbf{d}_{k,i}$ is generated randomly as

$$\mathbf{d}_{k,i} = \mathbf{d}_k + \mathbf{e}^o_{k,i},$$

where $\mathbf{e}^o_{k,i} \sim N(\mathbf{0}, \mathbf{R}_k)$.

To apply the Kalman filter, the error covariance matrix for the model is needed. In the Kalman filter this is defined in terms of the true state as the expectation

$$E((\Psi^{\mathrm{f}}_k - \Psi^{\mathrm{t}}_k)(\Psi^{\mathrm{f}}_k - \Psi^{\mathrm{t}}_k)).$$

Since the true state is not known, we approximate the true state by the mean of the ensemble

$$\Psi^{\mathrm{t}}_k \approx \widehat{\Psi^{\mathrm{f}}_k} = \frac{1}{N}\sum_{i=1}^{N} \Psi^{\mathrm{f}}_{k,i},$$

where N is the sample size of the ensemble. With this approximation of the true state, an approximation of a left factor of the error covariance matrix of the model is

$$\mathbf{L}^{\mathrm{f}}_k = \frac{1}{\sqrt{N}}\left[\left(\Psi^{\mathrm{f}}_{k,1} - \widehat{\Psi^{\mathrm{f}}_k}\right) \quad \left(\Psi^{\mathrm{f}}_{k,2} - \widehat{\Psi^{\mathrm{f}}_k}\right) \quad \ldots \quad \left(\Psi^{\mathrm{f}}_{k,N} - \widehat{\Psi^{\mathrm{f}}_k}\right)\right].$$

The approximation of the model error covariance matrix then becomes

$$\mathbf{P}^{\mathrm{f}}_k = \mathbf{L}^{\mathrm{f}}_k(\mathbf{L}^{\mathrm{f}}_k)^{\mathrm{T}}. \tag{11}$$

The expression of the Kalman gain matrix is (see e.g. Maybeck, 1979)

$$\mathbf{K}_k = \mathbf{P}^{\mathrm{f}}_k\mathbf{H}^{\mathrm{T}}(\mathbf{H}\mathbf{P}^{\mathrm{f}}_k\mathbf{H}^{\mathrm{T}} + \mathbf{R}_k)^{-1}.$$

The analyzed state of each member of the ensemble is computed as

$$\Psi^{\mathrm{a}}_{k,i} = \Psi^{\mathrm{f}}_{k,i} + \mathbf{K}_k(\mathbf{d}_{k,i} - \mathbf{H}\Psi^{\mathrm{f}}_{k,i}).$$

The analyzed error covariance matrix, $\mathbf{P}^{\mathrm{a}}_k$, of the model can be computed along the same lines as $\mathbf{P}^{\mathrm{f}}_k$. Since the updating of the ensemble is linear, the new estimate of the true state, based on the ensemble after the analysis step is

$$\Psi_k^{\mathrm{t}} \approx \widehat{\Psi_k^{\mathrm{a}}} = \widehat{\Psi_k^{\mathrm{f}}} + \mathbf{K}_k\left(\mathbf{d}_k - \mathbf{H}\widehat{\Psi_k^{\mathrm{f}}}\right),$$

and the model error covariance matrix after the analysis step is

$$\mathbf{P}_k^{\mathrm{a}} = (\mathbf{I} - \mathbf{K}_k\mathbf{H})\mathbf{P}_k^{\mathrm{f}}.$$

The underlying assumptions behind the filter are that there is zero covariance between the model error and the measurement error and that both the model error and measurement error are uncorrelated in time. For the practical implementation of the above procedure, it is important to bear in mind that while evaluating the Kalman gain matrix, $\mathbf{P}_k^{\mathrm{f}}$ should be entered factorized as in (11), and the product should be evaluated in an order such that the dimensions of temporary matrices are kept as low as possible.

4. Results

In this section we present and discuss examples which demonstrate the filter technique described above. Details regarding discretization, model error and measurement error are outlined in Sections 4.1–4.3. Section 4.4 contains two examples where two sets of model parameters are used to generate synthetic measurements. The ability to reconstruct the parameters by using the ensemble Kalman filter is then investigated, and forecasts using the estimated parameters are compared to the synthetic measurements. Section 4.5 contains an example where full-scale experimental measurements are used to tune the model parameters. A forecast of the two-phase flow is then compared to the measurements.

4.1. Discretization and state vector

Use of a numerical method requires a discretization of the time and space variables. We have used a spatial discretization where $\Delta s = 20$ m. Furthermore, a maximum value of 15 m/s is assumed for the gas velocity, which gives a maximum valid time-step $\Delta t = \Delta s/15\ \mathrm{s} \approx 1.3$ s.

By using the ensemble Kalman filter it is possible to combine the information obtained from the measurements with the model to get an improved estimation of the state vector. The state vector (Ψ) is composed of discretized pressure values and discretized gas and liquid mass rates. This is motivated by the fact that these variables are usually measured at some positions during drilling operations. The observation operator (**H**) is then composed by choosing the matrix which selects the values from the state vector corresponding to the measurements. In addition, the state vector includes several parameters from the closure relations related to drillstring and annulus. The state vector is then defined as

$$\Psi = [\,\mathbf{v} \quad \mathbf{p}\,]^{\mathrm{T}},$$

where

$$\mathbf{v} = [\,\cdots \quad p_J \quad F_{JR,g} \quad F_{JR,l} \quad \cdots\,]$$

and

$$\mathbf{p} = [\, C_{0,d} \quad C_{1,d} \quad C_{2,d} \quad C_{0,b} \quad C_{1,b} \quad C_{2,b} \quad C_{0,s} \quad C_{1,s} \quad C_{2,s} \,].$$

Here J indicates the cell number, p_J is the average pressure value of the cell, and $F_{JR,g}$ and $F_{JR,l}$ are the mass rate of gas and liquid, evaluated at the right cell wall.

4.2. Model error

The model error consists of both an initial error and an accumulating error term, with covariance matrixes $\mathbf{Q}_0$ and $\mathbf{Q}_k$ respectively. In this context we assume that the model error for the well flow variables $\mathbf{v}$ is accounted for by the uncertainty in the model parameters. This is done because the well flow parameters have notable impact on the flow behavior. The friction parameters influence the pressure gradient, while the slip parameters directly affect the flow velocities and flow rates. In addition, it is difficult to produce good estimates of the uncertainty of the discretized flow variables and the correlations which inevitably exist between them.

We assume $\mathbf{Q}_k$ to be time independent, and it can be written as

$$\{\mathbf{Q}\}_{ij} = \begin{cases} 0, & \text{if } i \neq j,\ i \text{ or } j \leqslant M \\ \epsilon, & \text{if } i = j \leqslant M \\ (\sigma_i^Q)^2, & \text{if } i = j > M \\ \sigma_i^Q \sigma_j^Q \rho_{ij}^Q, & \text{otherwise} \end{cases},$$

where M is the number of variables in $\mathbf{v}$, and ϵ is a small positive number (2.22×10^{-16}) which ensures that $\mathbf{Q}$ is positive definite. We note that ρ_{ij}^Q must be chosen in order to preserve positive definiteness. The matrix $\mathbf{Q}_0$ is expressed in the same manner.

The values ρ_{ij}^Q represent the correlation coefficients for the model errors related to the parameters. It is difficult to obtain accurate values for these correlations, and several values have been tried in the process leading to the results shown here. If no correlation between the parameters was assumed, we experienced cases where the parameters drifted towards unphysical values. This is due to the fact that parameters can counteract and several compositions can produce the same result. Based on this, we have chosen a common correlation $\rho_{ij}^Q = \rho_{ij}^{Q_0} = 0.85$ between all the parameters. (The value for these correlation coefficients is also based on experience resulting from the examples in Lorentzen et al., 2001a.) The consequences of this assumption is discussed further in Section 4.4.

As pointed out, the choice of the covariance matrix $\mathbf{Q}$, has great impact on the performance of the filter. Here we have demonstrated that a certain choice of $\mathbf{Q}$ give reasonable performance of the filter, but we have not tried to tune the the entries of the covariance matrix $\mathbf{Q}$ to optimize the performances. This is a topic for further research.

We also need to specify the expected initial state $\overline{\Psi_0^a}$ in Eq. (9). This is done by assuming that the well is initially filled with stagnant liquid and by using a set of predefined default model parameters. The predefined parameters are $\overline{C}_{0,d} = 1$ and $\overline{C}_{1,d} = -0.1$ for the parameters in Eq. (3), and $\overline{C}_{2,d} = 1$ in Eq. (4). For the parameters in the mechanistic model, we use the values as proposed by Lage and Time (2000). This gives an expected initial parameter vector

$$\overline{\mathbf{p}_0^a} = [\, 1 \quad -0.1 \quad 1 \quad 1 \quad 1 \quad 1 \quad 1.2 \quad 1 \quad 1 \,].$$

4.3. Measurement error

The covariance matrix $\mathbf{R}_k$ must be specified in order to apply the ensemble Kalman filter. In this context, we assume that measurement errors are uncorrelated. As done in Cohn (1997), the measurement error can be split into a term related to the measurement device and one term which is state-dependent due to a discretized numerical model (representativeness error). In Section 4.4 the pump pressure, bottom hole pressure and gas and liquid return rates are used as measured variables. In Section 4.5 measurements resulting from five pressure sensors in drillstring and annulus are used. We assume that flow rates and pump pressure are evaluated at the cell boundaries, and that representativeness error can be neglected for these values. The uncertainty is therefore only related to the measurement gauge. A value of 1% is adopted for the rate measurements, and 0.15% is used for the pump pressure.

Calculation of other pressure values are however subject to uncertainty in the numerical method, as this utilizes average pressure values. An interpolation is needed in order to gain the pressure values which corresponds to the measured values. There is also an uncertainty related to the position of the measurement gauge. We perform a simplified "worst case" analysis to obtain a value for the representativeness error. We assume that the pressure gauge is located in the middle of a grid box, and that the grid box is filled with 50% gas. If we neglect fluid velocities and pressure contribution due to the presence of gas, we get the following uncertainty in the pressure calculation

$$p^- < \bar{p} < p^+,$$

where $p^- = p_0$ is the pressure at the gauge position if all the gas in the grid box is located *above* the gauge, $\bar{p} = p_0 + \frac{1}{2}\rho_l g h$ is the output from the numerical method and $p^+ = p_0 + \rho_l g h$ is the pressure if all the gas is located *below* the pressure gauge, see Fig. 2. If we substitute data resulting from a 1000 m deep vertical well, discretized with 20 m grid boxes, we obtain an uncertainty of 0.5%. For simplicity, we use this value for all pressure measurements resulting from gauges in the interior well region.

4.4. Case 1—Synthetic generated measurements

By using synthetic generated measurements it is possible to compare estimated parameters and estimated physical state variables with a "true" solution. This gives a valuable validation of the filter, and indicates that it can be trusted when applied at real full-scale drilling operation where model error is caused by inaccuracies in the model parameters. In order to generate the mea-

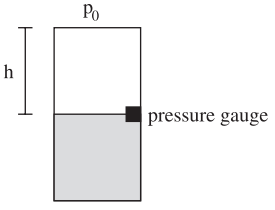

Fig. 2. Gas distribution in a grid box.

surements, the numerical method described in Section 2.3 is used to calculate a true state vector Ψ_k^{t} according to the equations

$$\Psi_k^{\mathrm{t}} = \mathbf{f}(\Psi_{k-1}^{\mathrm{t}}) + \widetilde{\mathbf{e}_k^m}$$

and

$$\Psi_0^{\mathrm{t}} = \overline{\Psi_0^{\mathrm{t}}} + \widetilde{\mathbf{e}_0^m}. \tag{12}$$

Eq. (10) is then used to calculate synthetic measurements representing pump pressure, bottom hole pressure and gas and liquid return rates. In this context, we use $\overline{\Psi_0^{\mathrm{t}}} = \overline{\Psi_0^{\mathrm{a}}}$. The error terms $\widetilde{\mathbf{e}_k^m}$ and $\widetilde{\mathbf{e}_0^m}$ are assumed to have the same distribution as $\mathbf{e}_{k,i}^m$ and $\mathbf{e}_{0,i}^m$, but possibly different correlation factors $\widetilde{\rho_{ij}^Q}$ and $\widetilde{\rho_{ij}^{Q_0}}$. In order to investigate the importance of these correlation factors, we show one example (Section 4.4.1) where measurements are generated by using the same correlation factors as in the Kalman filter equations (8) and (9), and one example (Section 4.4.2) where $\widetilde{\rho_{ij}^Q}$ and $\widetilde{\rho_{ij}^{Q_0}}$ are randomly distributed between 0 and 1. The motivation for adding stochastic noise to the true parameter values is to simulate external time varying effects caused by the surrounding environments and drilling equipment (e.g. change of fluid properties, flow variations and temperature variations). In both examples, we have chosen to run the simulator for 80 min, and sample the measurements every 60 s.

Based on experience, a value of 0.2 is chosen as initial standard deviation ($\sigma_i^{Q_0}$) for all parameters. A value of 5×10^{-3} is used as the accumulating error term (σ_i^{Q}). Note that this value depends upon how often the measurements are sampled.

We have chosen a dynamic test scenario where gas and liquid are injected (unloading) in two steps. The well configuration consists of a 1000 m deep vertical drillstring with a 6.03×10^{-2} m inner diameter, and an annulus with inner diameter equal to 8.89×10^{-2} m, and outer diameter equal to 1.59×10^{-1} m. The well is initially at rest and filled with water. Flow rates are increased to 4.25 Sm^3/min for gas and 400 l/min for liquid during a 60 s period. These rates are then kept constant in 40 min. The injection of gas in the drillstring causes the pump pressure to increase sharply, see the dashed curve in Fig. 3. At approximately 10 min gas enters the annulus and causes

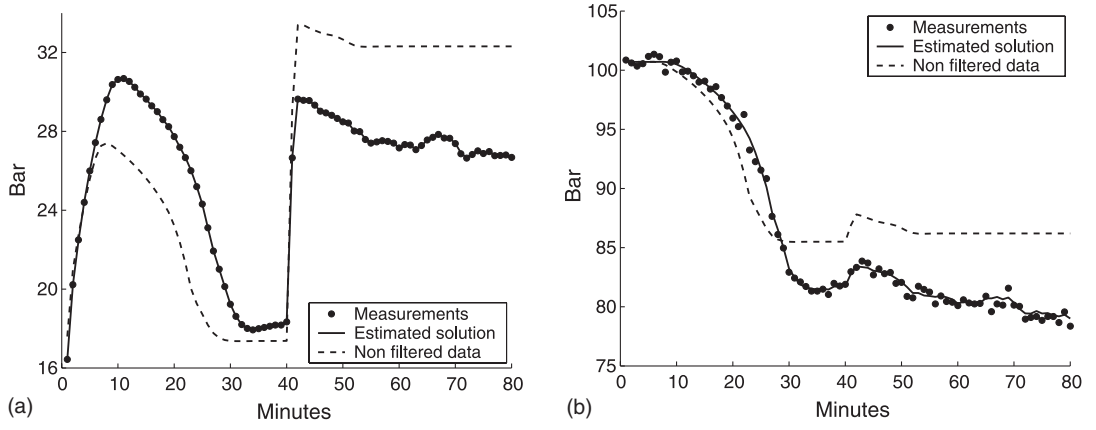

Fig. 3. The figure shows the pressure measurements in example 1, along with estimated data and a solution where the filter is not applied. (a) Pump pressue, (b) bottom hole pressure.

the bottom hole pressure to decrease. The gas front reaches the surface after approximately 25 min. At 40 min a new 60 s injection period starts, where the gas and liquid rates are doubled. The increase in mass rates generates higher frictional pressure loss. This results in a sudden increase in the pump pressure and the bottom hole pressure. At approximately 50 min a new gas front reaches the outlet.

4.4.1. Example 1—equal correlation

In this example the parameter correlation used to generate measurements is the same as in the Eqs. (8) and (9), that is $\widetilde{\rho_{ij}^{Q}} = \rho_{ij}^{Q}$ and $\widetilde{\rho_{ij}^{Q_0}} = \rho_{ij}^{Q_0}$. Eq. (12) is used to generate an initial true state, and in this case the resulting initial parameter vector is [1]

$$\mathbf{p}_0^{\mathrm{t}} = [0.80 \quad -0.30 \quad 0.82 \quad 0.88 \quad 0.83 \quad 0.75 \quad 1.08 \quad 0.81 \quad 0.76].$$

Figs. 3 and 4 show the measurements, the filtered solution and a solution where the filter is not applied. The non-filtered solution generated with $\overline{\mathbf{p}_0^{\mathrm{a}}}$, gives a solution which is different from the measurements, and spurious gas breakthrough and pressure values are calculated. This indicates the importance and need of accurate estimates of the parameter values. As the solid line indicates, the ensemble Kalman filter updates the well flow variables and better agreement with the measurements is obtained.

As the measurements are generated synthetically, it is possible to compare estimated and true flow variables which are not directly measured. Fig. 5 shows the estimated and true gas fraction at 500 m below sea surface in the drillstring and annulus. The figure shows good agreement between the estimated and true gas fraction, and indicates that the filter gives a good overall estimate of the well flow. As we will show below, the updated solution will to some degree remain in its new track, due to a simultaneous update of the parameter vector.

Figs. 6–8 show the evolution of parameter values. Note that the initial estimated parameters deviate slightly from their mean values $\overline{\mathbf{p}_0^{\mathrm{a}}}$, as they result from the mean of the initial (finite sized) ensemble. The initial leap towards the true parameter values is due to the initial model error which has a larger standard deviation than the accumulating error term. This causes the filter to trust the model less, and measurements more. An improvement in $C_{0,b}$ and $C_{0,s}$ is observed at approximately 30 min, see Figs. 7 and 8. At this time gas reaches the outlet where it is highly sensitive to variations in the model parameters. This causes the error covariance matrix for the forecasted state to increase, and the model will again be trusted less. In addition, the flow pattern becomes more complex as a transition regime and a slug flow regime are introduced at approximately 30 min, see Fig. 9. The estimation of the slug flow parameters has prior to this time been updated solely based upon the parameter correlations. The introduction of the transition and slug flow regime is due to increased presence of gas in annulus, which leads to a coalescence of the gas bubbles.

The filter will continuously exert to produce the best overall solution. This implies that the flow variables with the largest deviation from the measurements are improved, while possibly sacri-

[1] MATLAB™'s *randn*-function is used, which produces quasi-random numbers. The sequence of numbers generated is determined by the state of the generator. By storing this state, the numbers can be reproduced.

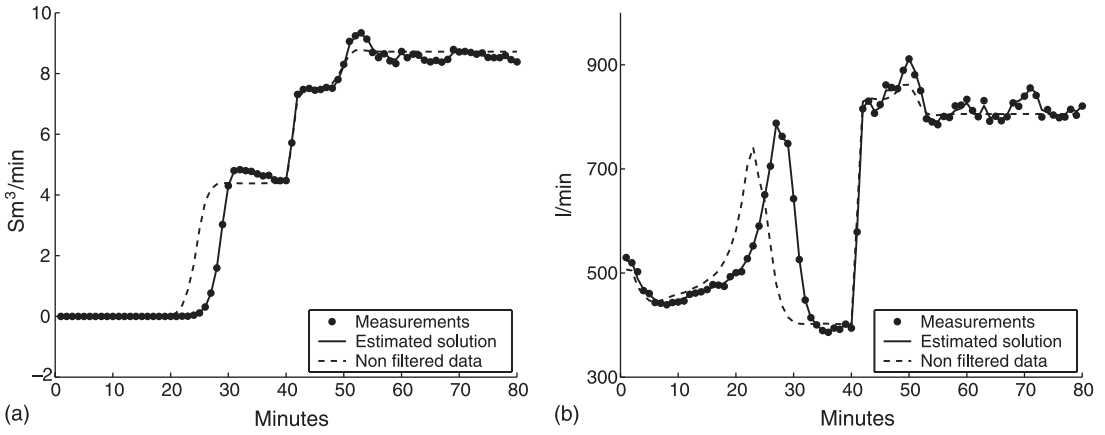

Fig. 4. The figure shows the rate measurements in example 1, along with estimated data and a solution where the filter is not applied. (a) Gas return rate, (b) liquid return rate.

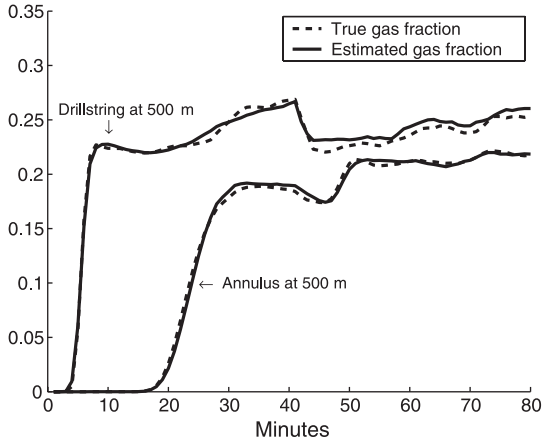

Fig. 5. True and estimated void fraction in example 1 at two different positions in the well.

ficing accuracy where the error is small. This is achieved by updating the parameters which have the largest influence on the solution. In the process of estimating the governing parameters, others might be withdrawn from their optimal value due to the correlation which exists between the parameters. This is probably the case for $C_{1,d}$ which tends to drift away as $C_{0,b}$ and $C_{0,s}$ approach their true values, see Fig. 6.

As the governing parameters approach the corresponding true values one can also expect the forecasted solution to better represent the measured data. We perform a forecast at 5 min, which illustrates the quality of the estimated solution when only a few measurements are taken into account. In addition, a forecast is performed at 30 min, which is prior to the dynamic behavior resulting from the second increase in the gas flow rate. Figs. 10 and 11 show the forecasts at these

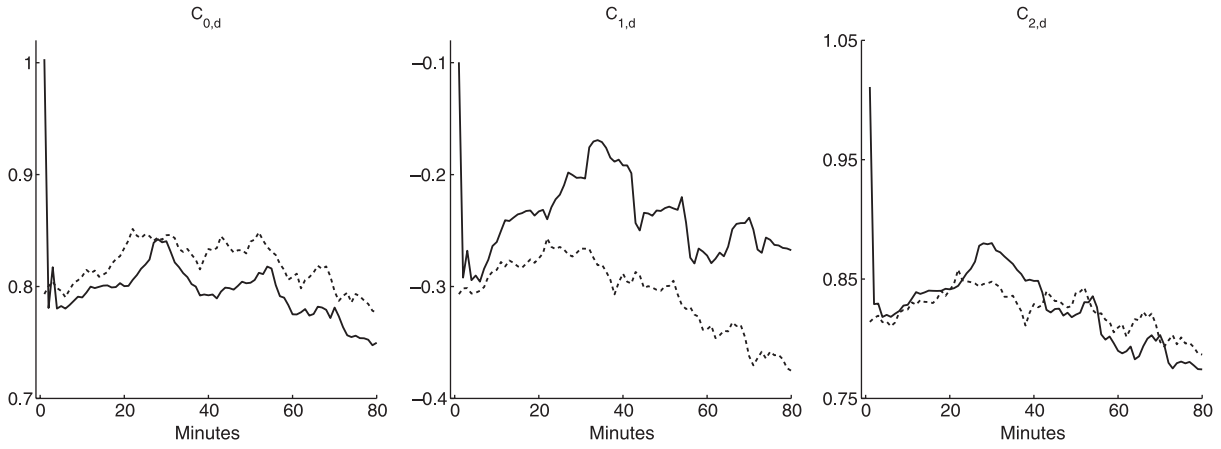

Fig. 6. Drillstring parameters in example 1. The dashed line represents the true value and the solid line represents the estimated value.

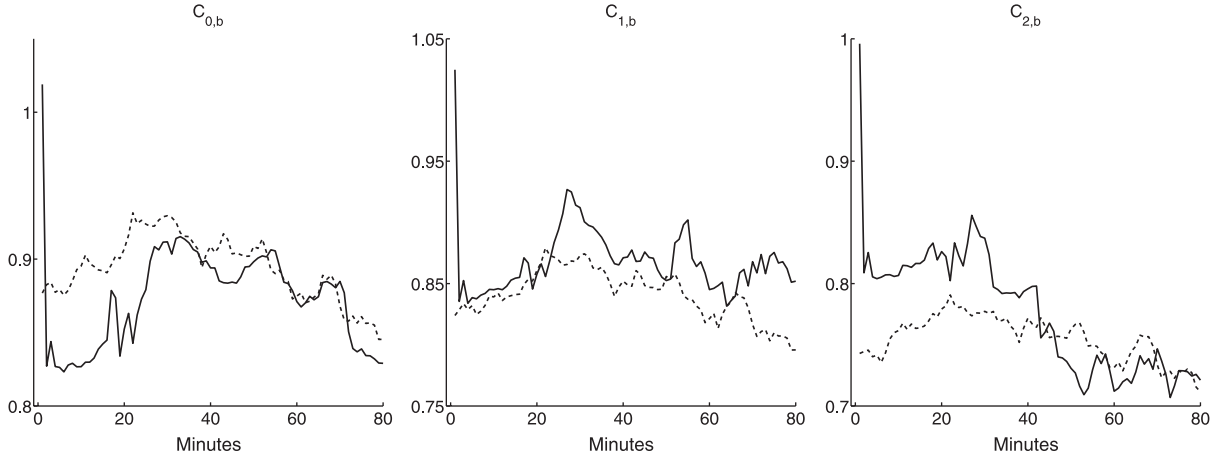

Fig. 7. Bubble flow parameters in example 1. The dashed line represents the true value and the solid line represents the estimated value.

moments. As the parameters are quickly improved due to the initial model error, the forecast solution starting from 5 min gives a considerable improvement when compared to the non-filtered solution. The pressure levels after the second injection are however underestimated, and the gas breakthrough is slightly displaced. The forecast starting from 30 min has reduced the deviation in the bottom hole pressure, and we believe this is due to a better estimate of $C_{0,s}$, see Fig. 8. The increase of this parameter has probably also caused an increase of parameter $C_{1,d}$, which results in a slightly overestimated pump pressure, see Fig. 10. The overall estimate is however improved compared to the forecast starting from 5 min.

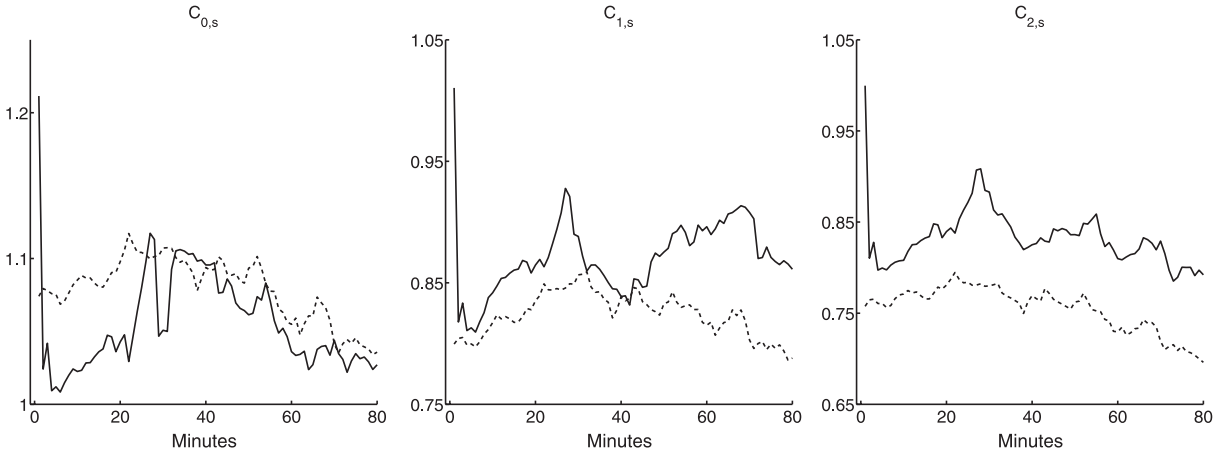

Fig. 8. Slug flow parameters in example 1. The dashed line represents the true value and the solid line represents the estimated value.

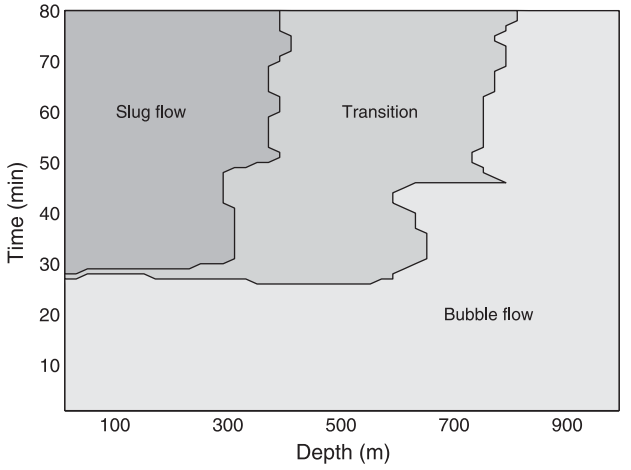

Fig. 9. Flow pattern in example 1.

4.4.2. Example 2—random correlation

In this example we show the parameter evolution and predicted solutions when the parameter correlations used to generate measurements are randomly distributed. We construct a positive definite correlation matrix Π according to

$$\Pi = \mathbf{D}^{-\frac{1}{2}}\mathbf{U}^{\mathrm{T}}\mathbf{U}\mathbf{D}^{-\frac{1}{2}},$$

where $\mathbf{U}$ is a upper triangular matrix consisting of random numbers between 0 and 1, and $\mathbf{D} = \mathrm{diag}(\mathbf{U}^{\mathrm{T}}\mathbf{U})$. In this particular case, the realization of $\mathbf{p}_0^{\mathrm{t}}$ is

$$\mathbf{p}_0^{\mathrm{t}} = [\,1.40 \quad 0.07 \quad 0.87 \quad 1.02 \quad 1.21 \quad 1.44 \quad 1.79 \quad 1.58 \quad 1.51\,].$$

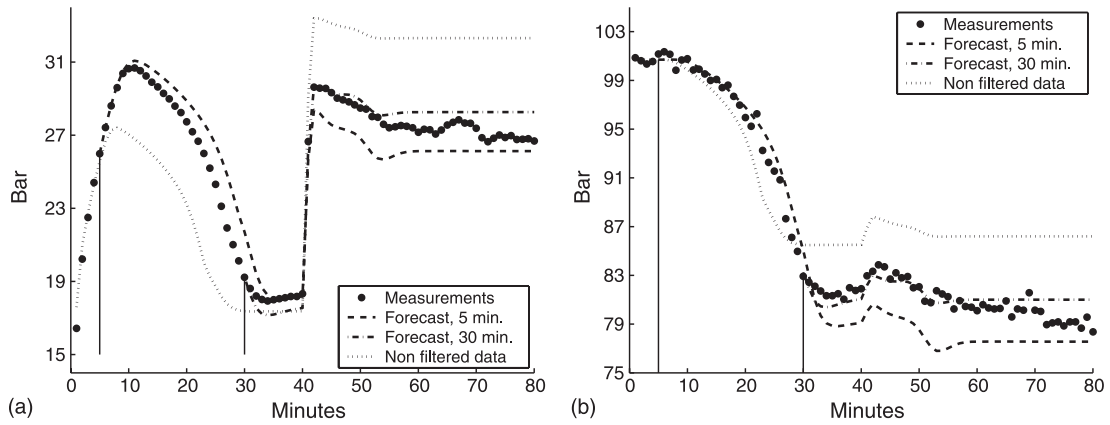

Fig. 10. The figures show predictions in example 1. The vertical lines indicate the start points at 5 and 30 min. (a) Pump pressue, (b) bottom hole pressure.

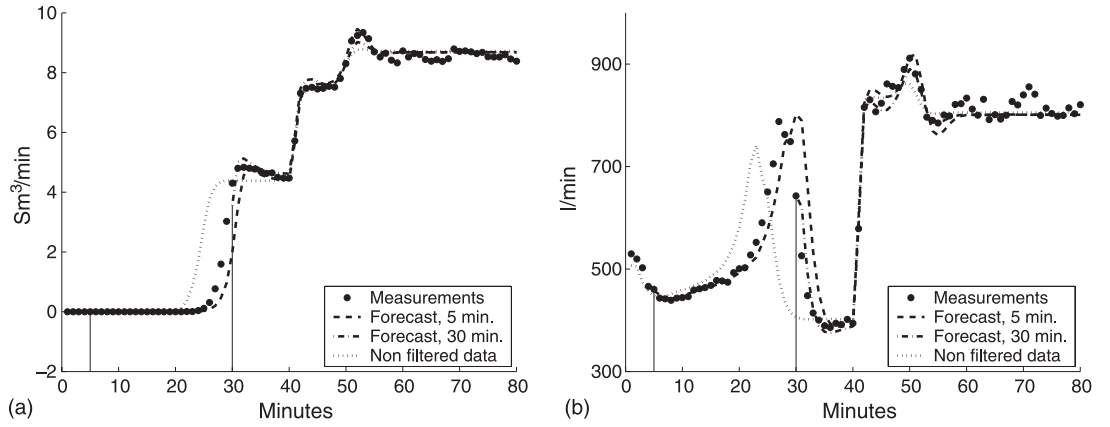

Fig. 11. The figures show predictions in example 1. The vertical lines indicate the start points at 5 and 30 min. (a) Gas return rate, (b) liquid return rate.

These parameters deviate very differently form the mean values. The parameter $C_{2,d}$ is e.g. more than 0.1 below its mean value, while $C_{0,s}$ is almost 0.6 above its mean value.

Figs. 12 and 13 show the measurements, the filtered solution and a solution where the filter is not applied. The physical flow variables are, as in Example 1, updated in accordance to the measurements. We observe that the true state is quite different when compared to the previous example. The pump pressure lies below the non-filtered solution, and the bottom hole pressure is approximately 7 bar too high at the steady state level. In addition, the gas breakthrough occur too late in the non-filtered solution.

The parameter evolution is shown in Figs. 14–16. Good results are obtained for most of the parameters, but the slug parameter is poorly estimated prior to the introduction of the slug regime (at approximately 30 min).

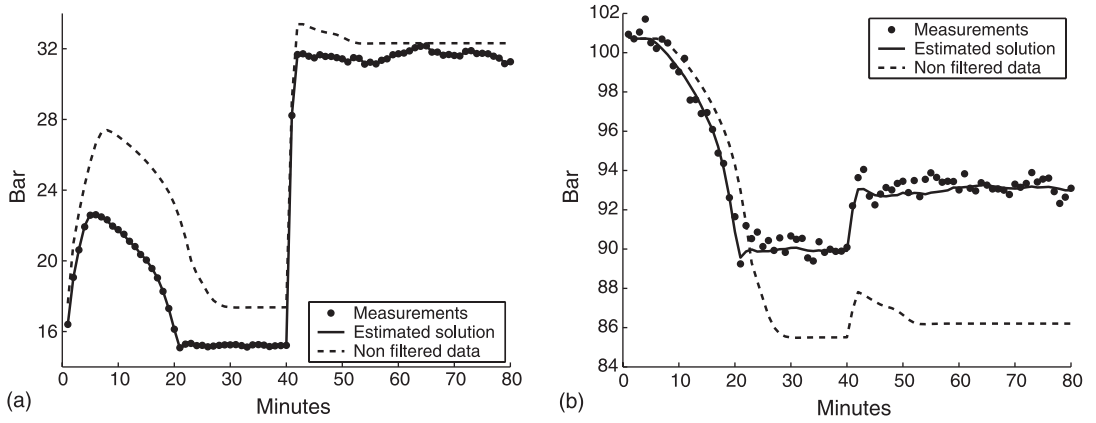

Fig. 12. The figure shows the pressure measurements in example 2, along with estimated data and a solution where the filter is not applied. (a) Pump pressue, (b) bottom hole pressure.

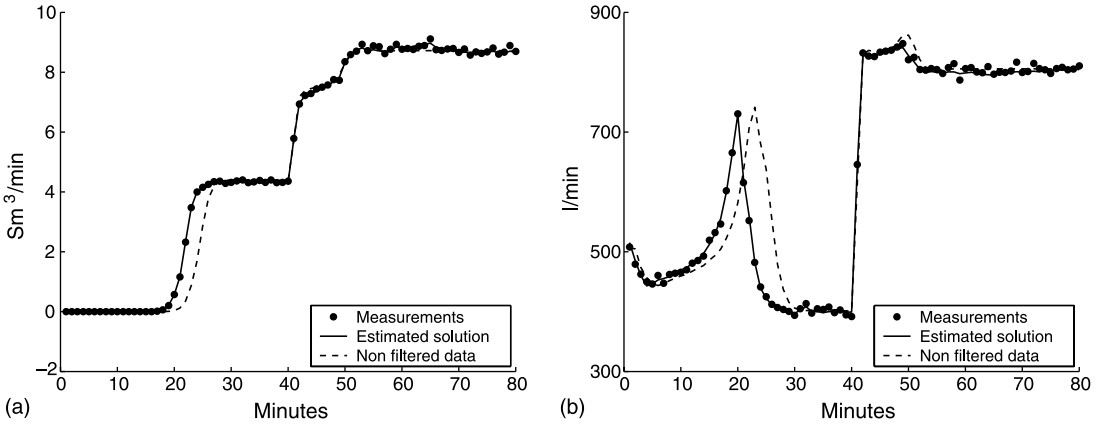

Fig. 13. The figure shows the rate measurements in example 2, along with estimated data and a solution where the filter is not applied. (a) Gas return rate, (b) liquid return rate.

Figs. 17 and 18 show that predictions from 5 min gives improvements, but the pressure measurements are not completely recovered. At 30 min the slug flow parameters are better estimated, and the well flow prediction is improved.

4.4.3. Conclusions

We have shown two examples where synthetic generated measurements are used to tune model parameters in the two-phase flow model. The measurements are generated using a set of "true" parameters, which is drawn from a Gaussian distribution. In Example 2, this distribution was not the same as in the Kalman filter setup. In Lorentzen (2002), two additional examples are shown. Here the correlation factors in the model error are respectively above and below the values used in the Kalman filter setup. As it is difficult to obtain accurate values for correlations between parameters, these results indicate that the ensemble Kalman filter possess the necessary robustness

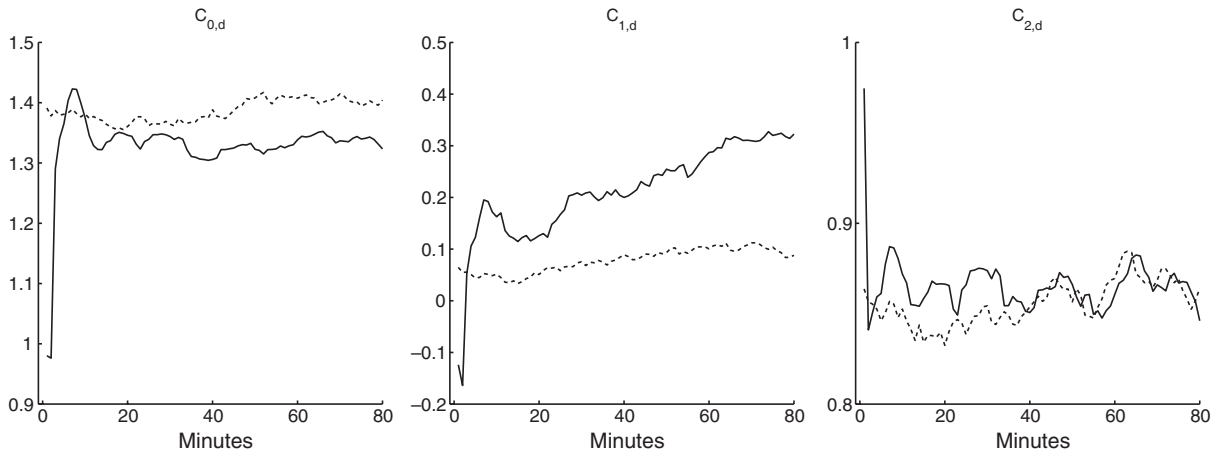

Fig. 14. Drillstring parameters in example 2. The dashed line represents the true value and the solid line represents the estimated value.

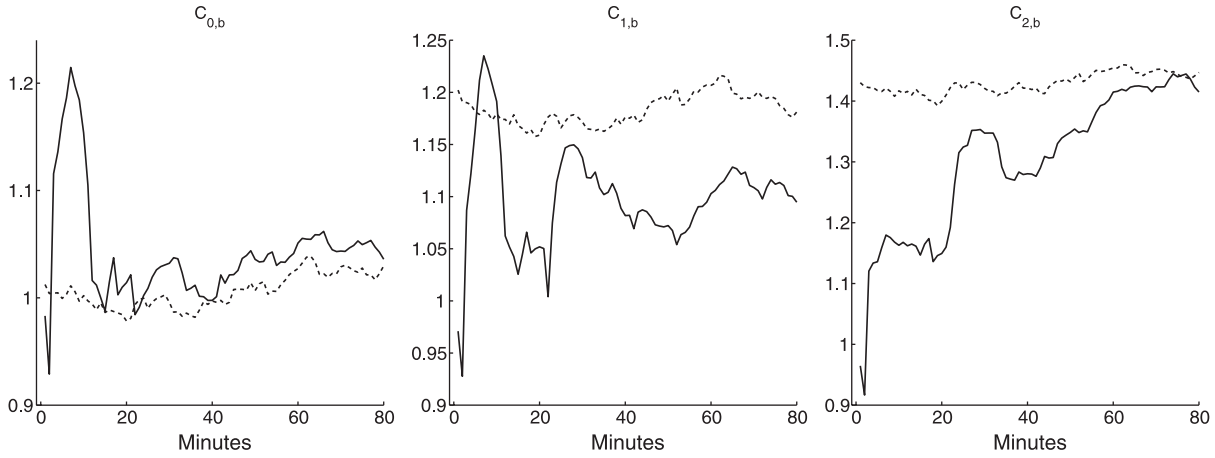

Fig. 15. Bubble flow parameters in example 2. The dashed line represents the true value and the solid line represents the estimated value.

for this application. In order to further test the filter, the next example uses a set of full-scale experimental measurements.

4.5. Case 2—full-scale experimental measurements

In this example the ability to track full-scale experimental measurements is illustrated. Fig. 19 shows a sketch of the experimental facility where the test was carried out. Four pressure-temperature sensors are disposed along the casing string in accordance to the sketch. The 6.5 in. drill bit with three orifices of 0.88 in. is placed at the bottom of the well at 1275 m of measured depth. The drill string and the casing constitute an 88.9 $\times$159.4 mm (3.5 $\times$6.3 in.) annular space. A wire

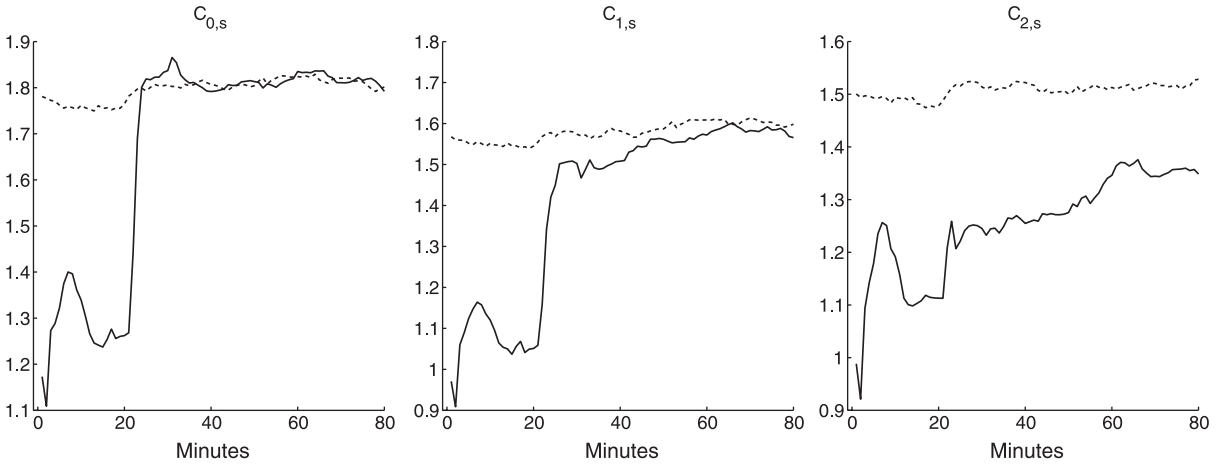

Fig. 16. Slug flow parameters in example 2. The dashed line represents the true value and the solid line represents the estimated value.

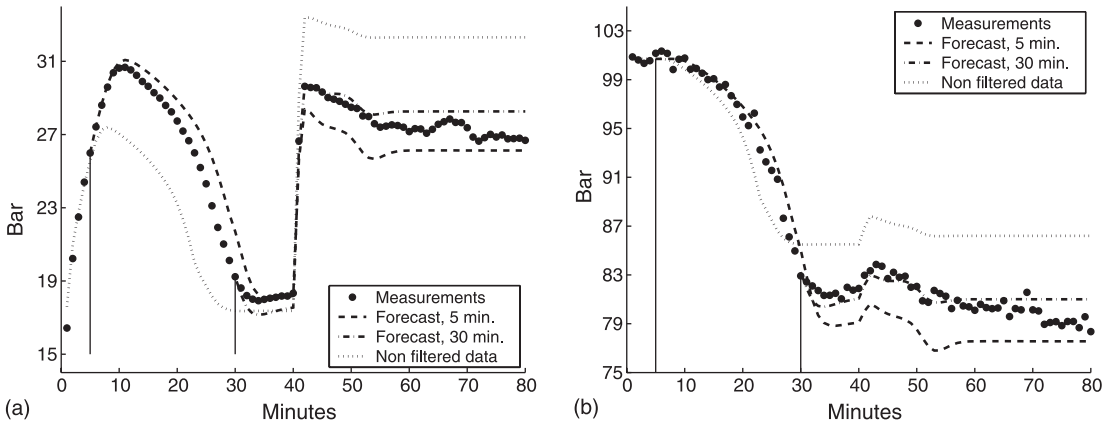

Fig. 17. The figures show predictions in example 2. The vertical lines indicate the start points at 5 and 30 min. (a) Pump pressue, (b) bottom hole pressure.

line logging tool is monitoring real time pressure and temperature in the drillstring at 490 m. In this context, the temperature measurements are neglected, and pressure measurements from four sensors in annulus and one sensor in drillstring are used. The measurements are sampled every 60 s, and a period of 180 min is simulated. The effect of variations in the sampling rate and reduction of available sensors are discussed in Lorentzen (2002).

In this example we have used 5×10^{-4} as standard deviation for the accumulating model error (σ_i^Q). A value of 1.5×10^{-3} is adopted as initial standard deviation ($\sigma_i^{Q_0}$). These values should reflect presumed uncertainty in the model parameters. It was however found necessary to restrict the standard deviations to some degree, to prevent too radical changes in the parameters from one

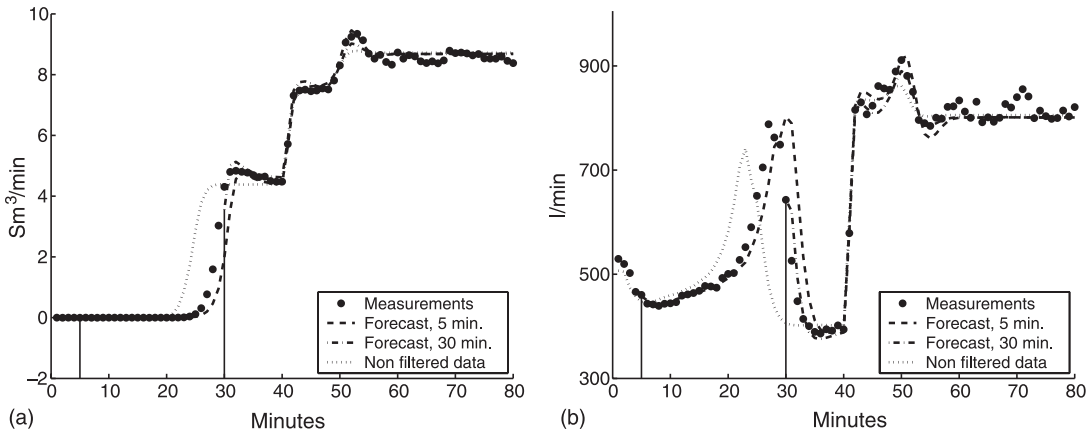

Fig. 18. The figures show predictions in example 2. The vertical lines indicate the start points at 5 and 30 min. (a) Gas return rate, (b) liquid return rate.

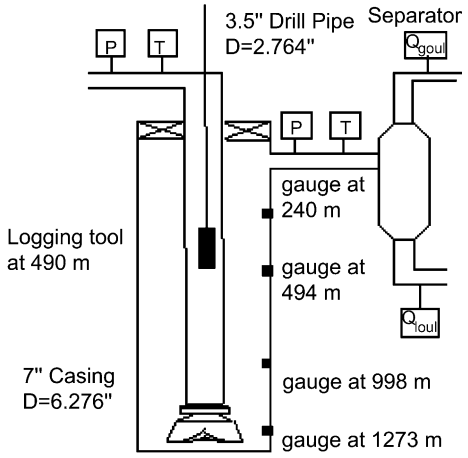

Fig. 19. Well configuration for the test facility.

time step to the next. If this happened, we experienced breakdowns in the simulator in periods where the flow is highly dynamic.

The tests start with the well at rest and filled with water, and the flow rates are increased to 7.6 Sm^3/min and 605.5 l/min for gas and liquid respectively. The injection of gas in the drillstring causes the pump pressure to increase sharply. At approximately 20 min the gas enters the annulus and causes the bottom hole pressure to decrease, see Fig. 24. The pressure sensors detect the presence of gas as the gas phase reaches their positions. After approximately 50 min of injection, the gas flow rate is adjusted to 15.2 Sm^3/min, while the liquid injection is kept at a constant rate. The increased presence of gas causes the bottom hole pressure to decrease with time. After 140 min, the gas rate is further increased to 25.4 Sm^3/min.

Figs. 20–22 show the measurements, the filtered solution and a solution where the filter is not applied. The model error is reduced when compared to Case 1, and the estimated solution is not following the measurements with the same accuracy as in that case. Improvements are however seen from approximately 30 min. As can be seen from the figures, the model is over-predicting the pressure throughout the well, and the (important) bottom hole pressure has at the most an error of 15 bar. The aim of applying the filter is to estimate parameters with higher validity for this well scenario, and thereby obtain more accurate forecasts of the flow.

The measurements show some pressure variations which are not present in the forecast solution (e.g. in the drillstring at approximately 100 min). These variations are due to complex choke constrains in the experimental facility, and these constrains are not included in the physical model used here. The focus in this case is therefore to capture the main tendencies of the two-phase flow.

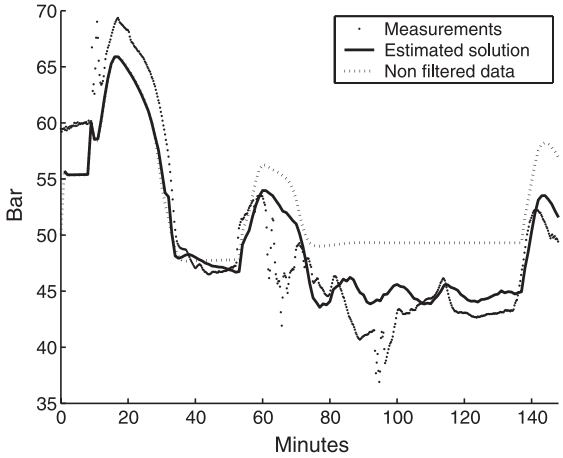

Fig. 20. The figure shows estimation of the drillstring pressure at 490 m. The measurements and an initial prediction are also shown.

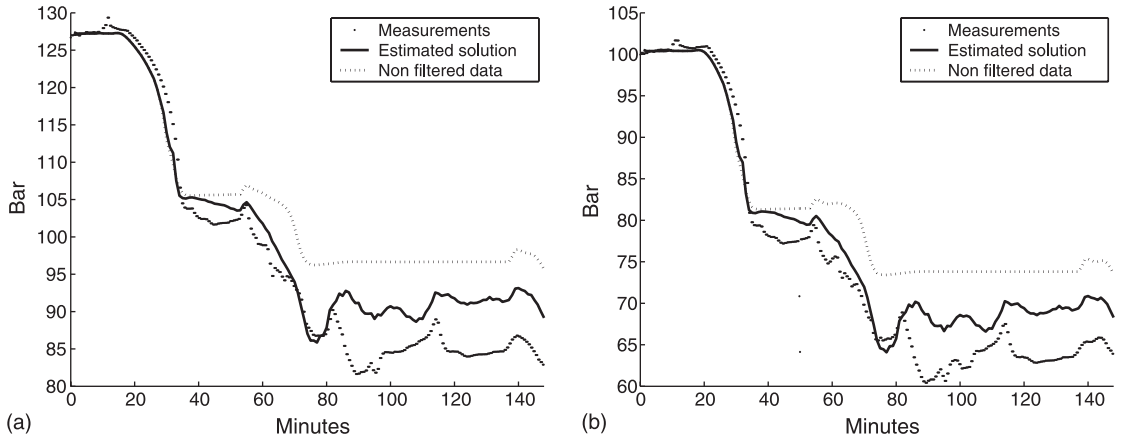

Fig. 21. The figures show estimations of the bottom hole pressure and the annulus pressure at 998 m. The measurements and an initial prediction are also shown. (a) Bottom hole pressure, (b) annulus pressure at 998 m.

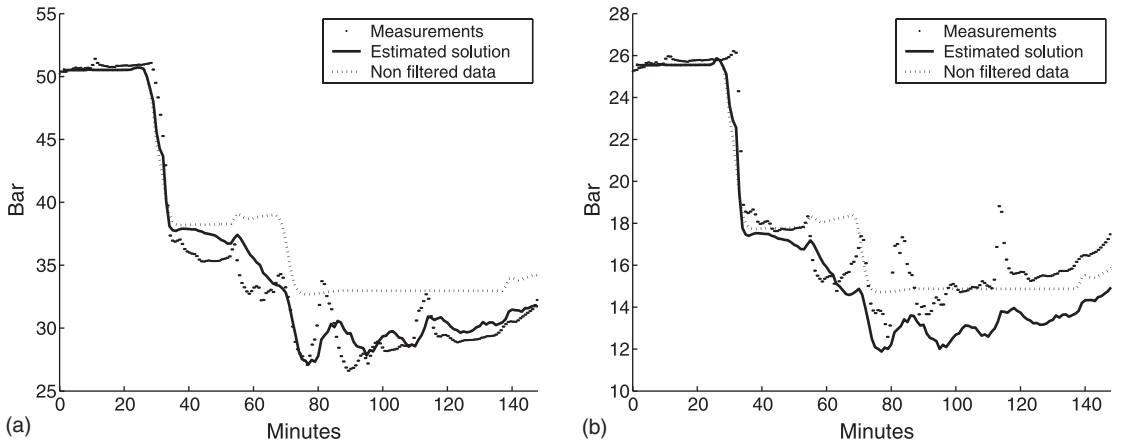

Fig. 22. The figures show estimations of the annulus pressure at 494 m and at 240 m. The measurements and an initial prediction are also shown. (a) Annulus pressure at 494 m, (b) annulus pressure at 240 m.

The state vector available at 60 min is used as initial state in the forecast of the two-phase flow. Table 1 shows a comparison between the estimated parameters and the parameters found in the literature. The estimated parameters are in this case reduced by approximately 0.1. This gives reduced friction pressure loss and gas velocity. The reduced gas velocity influences the hydrostatic pressure gradient, as more gas is accumulated in the system. The forecasts and measurements are

Table 1
Comparison of parameters found in literature and estimated parameters

	$C_{0,d}$	$C_{1,d}$	$C_{2,d}$	$C_{0,b}$	$C_{1,b}$	$C_{2,b}$	$C_{0,s}$	$C_{1,s}$	$C_{2,s}$
Default	−0.1	1	1	1	1	1	1.2	1	1
Estimated	−0.2	0.9	1.02	0.87	0.9	0.88	1.11	0.87	0.9

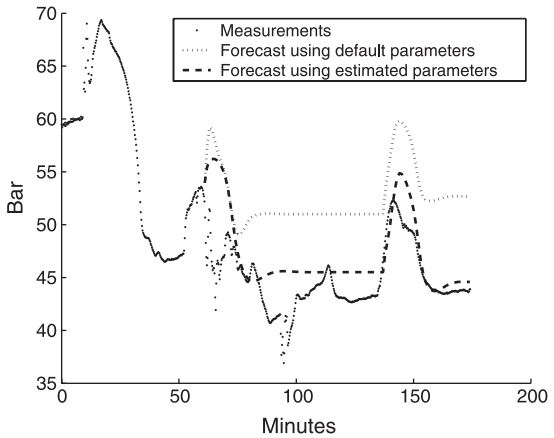

Fig. 23. The figure shows prediction of the drillstring pressure at 490 m.

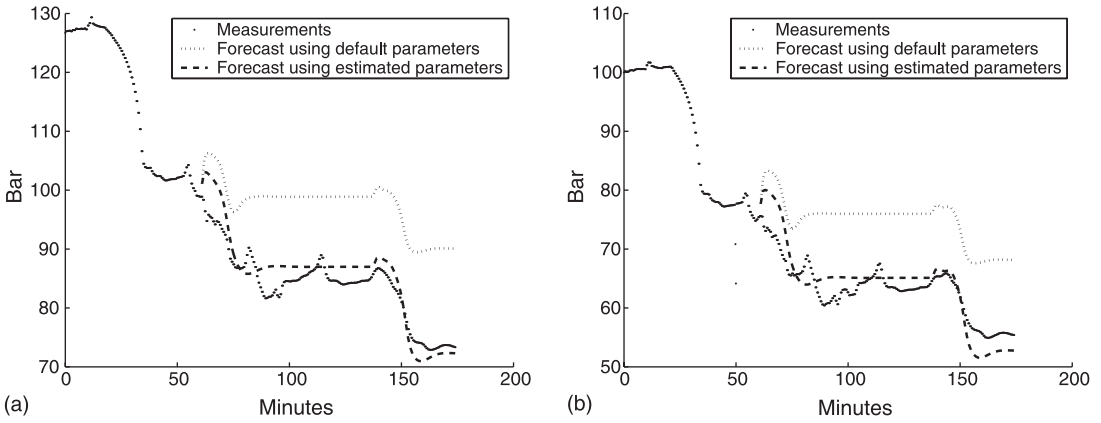

Fig. 24. The figures show predictions of the bottom hole pressure and the annulus pressure at 998 m. (a) Bottom hole pressure, (b) annulus pressure at 998 m.

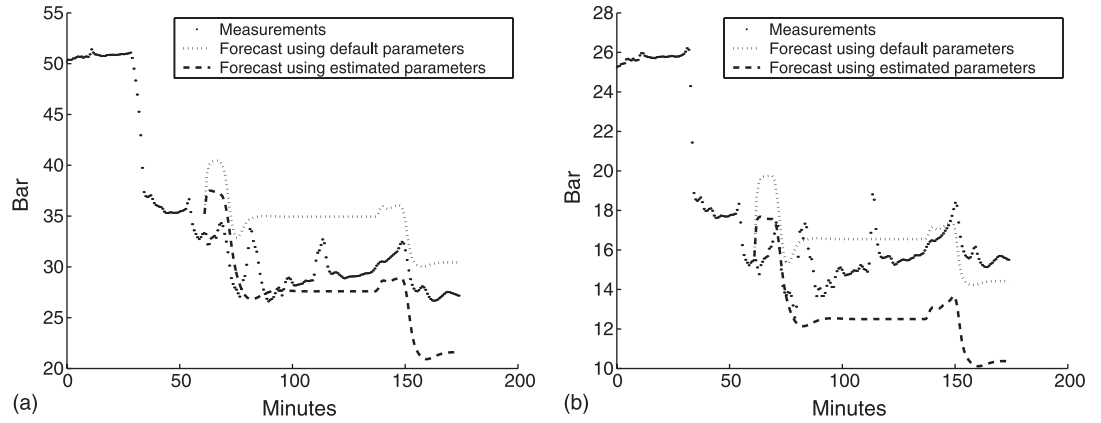

Fig. 25. The figures show predictions of the annulus pressure at 494 m and at 240 m. (a) Annulus pressure at 494 m, (b) annulus pressure at 240 m.

shown in Figs. 23–25. The figures also show a forecast where the estimated physical variables ($\mathbf{v}$) is used as an initial condition, but the default parameters are still kept. This forecast shows that is is crucial to update the model parameters, as the well flow in this case quickly approaches the solution obtain without the filter (compare with the non-filtered data shown in Figs. 20–22). The forecast using estimated parameters show large improvements at the sensor position in the drillstring and at the two deepest positions in the annulus. At the positions close to the outlet, the predictions are drifting away from the optimal track. This is due to the fact that largest difference between model and measurements occur at positions where the pressure is high. Measurements at these positions does therefore obtain a larger weight in the Kalman filter equations, and parameters are tuned so that better agreement is achieved. Accurate prediction of the bottom hole pressure is however considered to be of particular interest during several operations related to drilling and production.

5. Summary and conclusions

A new approach of tuning of parameters in two-phase flow models is presented. The approach uses an ensemble Kalman filter in the tuning. Motivated by applications in underbalanced drilling, the modeling of two-phase flow in wells is outlined and the implementation of the ensemble Kalman filter is presented. We have shown one way of including model parameters in the filter and present two studies of the suggested approach.

First, we study the robustness of the method using synthetic data. Synthetic measurements are generated by running the simulator using different sets of model parameters. Although the model parameters are not correctly recovered, the filter produce solutions which fits the observations and give improved forecasts compared to using the standard choice of model parameters. As this holds for different choices of "true" model parameters, this leads us to conclude that the ensemble Kalman filter approach has necessary robustness properties for this application.

The second study applies the suggested approach to experimental data. It is shown that tuning the chosen model parameters gives a solution which improved fitting of the measurements, and the forecast is significantly better than the solution obtained without the filter. Still there are some behavior of the flow which the filter is not able to track. This points to the fact that there are challenges ahead both on the modeling of the process and in the use of the Kalman filter techniques for online model parameter tuning.

Acknowledgements

We thank the Norwegian Research Council for financial support through the Strategic Institute Program "Complex Wells". We also thank our colleagues at RF-Rogaland Research, Erlend H. Vefring, Kjell K. Fjelde, Ove Sævareid and Johnny Frøyen, for useful discussions.

References

Anderson, J.L., 2001. An ensemble adjustment Kalman filter for data assimilation. Monthly Weather Rev. 129, 2884–2903.

Bendiksen, K., 1984. An experimental investigation of the motion of long bubbles in inclined tubes. Int. J. Multiphase Flow 10, 467–483.

Bendiksen, K., Malnes, D., Moe, R., Nuland, S., 1991. The dynamic two-fluid model OLGA: Theory and application. SPE Production Engineering.

Bendiksen, K.H., Malnes, D., Nydal, O.J., 1996. On the modelling of slug flow. Chem. Eng. Comm. 141–142, 71–102.

Burgers, G., van Leeuwen, P.J., Evensen, G., 1998. On the analysis scheme in the ensemble Kalman filter. Mon. Weather Rev. 126, 1719–1724.

Cassaude, B., Fabre, J., Jean, C., Ozon, P., Theron, B., June 1989. Unsteady phenomena in horizontal gas–liquid slug flow. In: Proceedings of the 4th International Conference on Multi-phase Flow. Nice, France, Cranfield, BHRA , pp. 469–484.

Cohn, S.E., 1997. An introduction to estimation theory. J. Meteorolog. Soc. Jpn. 75, 257–288.

Evensen, G., 1994. Sequential data assimilation with a nonlinear quasi-geostrophic model using Monte Carlo methods to forecast error statistics. J. Geophys. Res. 99, 10143–10162.

Faille, I., Heintzé, E., 1999. A rough finite volume scheme for modeling two-phase flow in a pipeline. Computers & Fluids, 213–241.

Fjelde, K.K., 2000. Numerical schemes for complex nonlinear hyperbolic systems of equations. Ph.D. thesis, Department of Mathematics, University of Bergen.

Franca, F., Lahey, R., 1992. The use of drift-flux techniques for the analysis of horizontal 2-phase flows. Int. J. Multiphase Flow 18, 787–801.

Frøyen, J., Sævareid, O., Vefring, E.H., 2000. Discretization, implementation and testing of a semi-implicit method. Tech. rep., RF— Rogaland Research, confidential.

Gavage, S.B., 1991. Analyse numérique des modèles hydrodynamiques d'écoulements diphasiques instationnaires dans les réseaux de production pétrolière. Thèse, ENS Lyon France.

Hamil, T.M., Whitaker, J.S., Snyder, C., 2001. Distance-dependent filtering of background error covariance estimates in an ensemble Kalman filter. Monthly Weather Rev. 129, 2776–2790.

Harmathy, T., 1960. Velocity of large drops and bubbles in media of infinite or restricted extent. AIChE J. 6, 281–288.

Houtekamer, P.L., Mitchell, H.L., 1998. Data assimilation using an ensemble Kalman filter technique. Monthly Weather Rev. 126, 796–811.

Ishii, M., 1975. Thermo-Fluid Dynamic Theory of Two-Phase Flow. Eyrolles, Paris.

Kelessidis, V., Dukler, A., 1989. Modeling flow pattern transitions for upward gas–liquid flow in vertical concentric and eccentric annuli. Int. J. Multiphase Flow 15, 173–191.

Lage, A.C.V.M., 2000. Two-phase flow models and experiments for low-head and underbalanced drilling. Ph.D. thesis, Stavanger University College, Norway.

Lage, A.C.V.M., Time, R.W., October 2000. Mechanistic model for upward two-phase flow in annuli. In: The 2000 SPE Annual and Technical Conference and Exhibition. Dallas, Texas, SPE 63127.

Lage, A.C.V.M., Fjelde, K.K., Time, R.W., September 2000a. Underbalanced drilling dynamics: Two-phase flow modeling and experiments. In: The 2000 IADC/SPE Asia Pacific Drilling Technology. Kuala Lumpur, Malaysia, IADC/SPE 62743.

Lage, A.C.V.M., Frøyen, J., Sævareid, O., Fjelde, K.K., October 2000b. Underbalanced drilling dynamics: Two-phase flow modeling, experiments and numerical solution techniques. In: The Rio Oil & Gas Conference. Rio de Janerio, Brazil, IBP 41400.

Lorentzen, R.J., April 2002. Higher order numerical methods and use of estimation techniques to improve modeling of two-phase flow in pipelines and wells. Ph.D. thesis, Department of Mathematics, University of Bergen.

Lorentzen, R.J., Fjelde, K.K., Frøyen, J., Lage, A.C.V.M., Nævdal, G., Vefring, E.H., 30 September–3 October 2001a. Underbalanced and low-head drilling operations: Real time interpretation of measured data and operational support. In: 2001 SPE Annual Technical Conference and Exhibition. SPE 71384.

Lorentzen, R.J., Fjelde, K.K., Frøyen, J., Lage, A.C.V.M., Nævdal, G., Vefring, E.H., 27 February–1 March 2001b. Underbalanced drilling: Real time data interpretation and decision support. In: SPE/IADC Drilling Conference. Amsterdam, The Netherlands, SPE/IADC 67693.

Maybeck, P.S., 1979. In: Stochastic models, estimation, and control, Vol. 1. Academic Press, New York.

Nævdal, G., Mannseth, T., Vefring, E.H., 3–6 September 2002a. Instrumented wells and near-well reservoir monitoring through ensemble Kalman filter. In: Proceedings of 8th European Conference on the Mathematics of Oil Recovery. Freiberg, Germany.

Nævdal, G., Mannseth, T., Vefring, E.H., April 2002b. Near-well reservoir monitoring through ensemble Kalman filter. In: SPE/DOE Improved Oil Recovery Symposium. Tulsa, Oklahoma, SPE 75235.

Papadimitriou, D., Shoham, O., April 1991. A mechanistic model for predicting annulus bottomhole pressures in pumping wells. In: 1991 Production Operations Symposium. Oklahoma City, SPE 21669.

Pauchon, C.L., Dhulesia, H., Binh-Cirlot, G., Fabre, J., September 1994. Tacite: A transient tool for multiphase pipeline and well simulation. In: The 1994 SPE Annual and Technical Conference and Exhibition. New Orleans, LA, SPE 28545.

Taitel, Y., Barnea, D., 1983. Counter current gas–liquid vertical flow, model for flow pattern and pressure drop. Int. J. Multiphase Flow 9, 637–647.

Théron, B., 1989. Ecoulements diphasique instationnaires en conduite horizontale. Thèse, INP Toulouse, France.

Verlaan, M., Heemink, A.W., 2001. Nonlinearity in data assimilation applications: A practical method for analysis. Monthly Weather Rev. 129, 1578–1589.

Wallis, G., 1969. One Dimensional Two-Phase Flow. McGraw-Hill Book Co. Inc.